Supporting Information

S1 Table. Table of plasmids used in this study.

Name	Origin of replication	Marker	Promoter	Gene(s) of interest	Description	Reference
pKD46	repA101ts	AmpR	pAraB	*gam, bet, exo*	Temperature sensitive plasmid containing the Phage λ Red recombination system	(Datsenko & Wanner, 2000)
pCP15	pMB1	AmpR, Kan R		*FRT-KanR-FRT*	Kanamycin resistance cassette flanked by FRT sequences	(Cherepanov & Wackernagel, 1995)
pCP16	pMB1	AmpR, Tet R		*FRT-tetAR-FRT*	TetRacycline resistance cassette flanked by FRT sequences	(Cherepanov & Wackernagel, 1995)
pCP20	repA101ts	AmpR, Cm R		*flp*	Temperature sensitive plasmid expressing the FLP recombinase ("flippase")	(Cherepanov & Wackernagel, 1995)
pTU136	R6K	AmpR	pLac	*ssdsbA-mCherry*	Template for mCherry gene sequence	(Uehara, Dinh, & Bernhardt, 2009)
pYSD1003	pMB1	AmpR		*sfYFP*	Template for super-folder mYFP gene sequence	This study
pYSD1004	pMB1	AmpR		*sfCFP*	Template for super-folder mCFP gene sequence	This study
pYSD1011	pMB1	KanR	pBla	*sfCFP*	mCFP under the control of the *bla* promoter from pUC19	This study
pYSD1007	pMB1	AmpR, Kan R	pLac	*cheB-mYFP*	Template for the translational fusion of CheB and mYFP	This study
pYSD1005	pMB1	AmpR, Kan R	pLac	*mCherry-cheR*	Template for the translational fusion of mCherry and CheR	This study

S2 Table. Table of bacterial strains used in this study.

Name	Description	Reference
RP437	Wild-type for chemotaxis	(Parkinson, 1978)
RP4972	ΔcheB	(Parkinson, 1978)
NWF121	ΔcheRcheB-FRT with ~300 bp CheB 3' fragment	This study
YSD2023	pLac-mCherry-cheR, FRT-kanR-FRT	This study
YSD2024	pRha-mCherry-cheR, FRT-kanR-FRT	This study
YSD2025	pLac-cheB-mYFP, FRT-kanR-FRT	This study
YSD2027	pRha-cheB-mYFP, FRT-kanR-FRT	This study
YSD2031	pBla-mCFP, FRT-kanR-FRT	This study
YSD2040	ΔcheRcheB, FRT, pLac-cheB-mYFP, FRT	This study
YSD2041	ΔcheRcheB, FRT, pLac-mCherry-cheR, FRT	This study
YSD2044	ΔcheB, pLac-cheB-mYFP, FRT	This study
YSD2062	ΔcheRcheB, FRT, pLac-cheB-mYFP, FRT, pRha-mCherry-cheR, FRT	This study
YSD2063	ΔcheRcheB, FRT, pRha-cheB-mYFP, FRT, pLac-mCherry-cheR, FRT	This study
YSD2072	ΔcheRcheB, FRT, pLac-cheB-mYFP, FRT, pRha-mCherry-cheR, FRT, pBla-mCFP, FRT	This study
YSD2073	ΔcheRcheB, FRT, pRha-cheB-mYFP, FRT, pLac-mCherry-cheR, FRT, pBla-mCFP, FRT	This study

S3 Table. Table of oligonucleotides primers used in this study.

Construct	Primer name	Sequence	Template	Product
pYSD1011	PUC19_PBLA_SYNTH_FOR	CATACTCTTCCTTTTTCAATATTATTG	pUC19	Vector backbone
	PUC19_BLA_SYNTH_REV	TAAGCATTGGTAACTGTCAGAC		
	PUC_PBLA_MYFP_N	CAATAATATTGAAAAAGGAAGAGTATGGTGAGCAAGGGCGAGGAG	pYSD1004	mCFP
	FRT_N - MYFP_C	CGGGTACCGAGCTCGAATTCTTACTTGTACAGCTCGTCCATGCC		
	FRT-N	GAATTCGAGCTCGGTACCCG	pCP15	FRT-kanR-FRT
	PUC_BLA_FRT_C	GTCTGACAGTTACCAATGCTTAAAGCTTCAAAAGCGCTCTGA		
pYSD1007	PUC19UNIV-SYNTHESISNONOT1 FOR	GATCCTCTAGAGTCGACCTG	pUC19	Vector backbone
	PUC19UNIV-SYNTHESISNONOT1 REV	CGGGTACCGAGCTCGAATTC		
	PUC19 - CHEB	CAGGTCGACTCTAGAGGATCATGAGCAAAATCAGGGTGTTATCTG	*E. coli* RP437	cheB
	LINKER_CHEB-C	GGAACCTCCACCGCCAATACGTATCGCCTGTCCGG		
	CHEB-C_LINKER_MYFP-N	CCGGACAGGCGATACGTATTGGCGGTGGAGGTTCCGTGAGCAAGG GCGAGGAG	pYSD1003	mYFP
	FRT_N - MYFP_C	CGGGTACCGAGCTCGAATTCTTACTTGTACAGCTCGTCCATGCC		
	FRT-N	GAATTCGAGCTCGGTACCCG	pCP15	FRT-kanR-FRT
	PUC19 - FRT	GAATTCGAGCTCGGTACCCGAAGCTTCAAAAGCGCTCTGA		
pYSD1005	PUC19UNIV-SYNTHESISNONOT1 FOR	GATCCTCTAGAGTCGACCTG	pUC19	Vector backbone
	PUC19UNIV-SYNTHESISNONOT1 REV	CGGGTACCGAGCTCGAATTC		
	PUC19 - MYFP	CAGGTCGACTCTAGAGGATCATGGTGAGCAAGGGCGAGGAG	pTU136	mCherry
	CHER-N_LINKER_MYFP-C	CCCACAGGGCAGAGATGAAGTGCCGCCGCCGCCGCCCTTGTACA GCTCGTCCATGCC		
	LINKER_CHER-N	GGCGGCGGCGGCGGCACTTCATCTCTGCCCTGTGGG	*E. coli* RP437	cheR
	FRT-N_CHER-C	CGGGTACCGAGCTCGAATTCTTAATCCTTACTTAGCGCATACAC		
	FRT-N	GAATTCGAGCTCGGTACCCG	pCP15	FRT-kanR-FRT
	PUC19 - FRT	GAATTCGAGCTCGGTACCCGAAGCTTCAAAAGCGCTCTGA		
NWF121	CHER_TETF	CATGAAGTAGCACGACATGAGTCGGTGCAGTTACAAATTGCGCC AGTGGTATCCTGAAGTGATTGAGAAGGCGCTATGACTTCATCTC TGTGCCACCTGACGTCTAAGAA	pCP16	FRT-tetAR-FRT
	CHEBALT_TETR	GTTAACCGCCGGGCCATCGTGAATTTTGATTTGGTAATTTGCGC CACTACGCGACAGCTCCATATGCCGATCGCCCGGCGCAATATAG GCTTTGCGCATTCACAGTTCTC		
YSD2023	PLAC-MYFP	TATGTTGTGTGGAATTGTGAGCGGATAACAATTTCACACAGGAA ACAGCTATGGTGAGCAAGGGCGAGGAG	pYSD1005	pLac-mCherry-CheR-FRT-kanR-FRT-lacZ'
	LACZ-C_FRT	TTATTTTTGACACCAGACCAACTGGTAATGGTAGCGACCGGCGC TCAGCTAAGCTTCAAAAGCGCTCTGA		
YSD2024	PRHA-MYFP	ATTCAGGCGCTTTTTAGACTGGTCGTAATGAAATTCAGCAGGAT CACATTATGGTGAGCAAGGGCGAGGAG	pYSD1005	pRha-mCherry-CheR-FRT-kanR-FRT-rhaA'
	RHAA-C_FRT	TTACCCGCGGCGACTCAAAATTTCTTTCTCATAAGCCCGCACGC TCTCCAAAGCTTCAAAAGCGCTCTGA		
YSD2025	PLAC-CHEB	TATGTTGTGTGGAATTGTGAGCGGATAACAATTTCACACAGGAA ACAGCTATGAGCAAAATCAGGGTGTTATCTG	pYSD1007	pLac-CheB-mYFP-FRT-kanR-FRT-lacZ'
	LACZ-C_FRT	TTATTTTTGACACCAGACCAACTGGTAATGGTAGCGACCGGCGC TCAGCTAAGCTTCAAAAGCGCTCTGA		
YSD2027	PRHA-CHEB	ATTCAGGCGCTTTTTAGACTGGTCGTAATGAAATTCAGCAGGAT CACATTATGAGCAAAATCAGGGTGTTATCTG	pYSD1007	pRha-CheB-mYFP-FRT-kanR-FRT-rhaA'
	RHAA-C_FRT	TTACCCGCGGCGACTCAAAATTTCTTTCTCATAAGCCCGCACGC TCTCCAAAGCTTCAAAAGCGCTCTGA		
YSD2031	ARAA_PUC_PBLA	TAGCGACGAAACCCGTAATACACTTCGTTCCAGCGCAGCGCGTC TTTAAATCTCAGTACAATCTGCTCTGA	pYSD1011	araA'-pBla-mCFP-FRT-kanR-FRT-araB'
	ARAB_PUC_BLA	GGCGATGAGCGCCGAACAACACTATCTTCCAACTTCCGCCCCGG CACAGGAACTTGGTCTGACAGTTACCA		

S4 Table. Table of model parameters used in this study.

Receptor Parameters			
Name	**Description**	**Value**	**Reference**
ε_1	Receptor energy change per methyl group addition	-1 k_BT	Shimizu et al. 2010
Signaling Parameters			
Name	**Description**	**Value**	**Reference**
k_r	Catalytic rate of CheR	0.42 s^{-1}	Frankel et al., 2014
K_r	Equilibrium constant of CheR activity	1200 μM	Frankel et al., 2014
k_b	Catalytic rate of CheB demethylation	0.32 s^{-1}	Frankel et al., 2014
k_Q	Catalytic rate of CheB deamination	0.64 s^{-1}	*this study*
K_b	Equilibrium constant of CheB activity	800 μM	Frankel et al., 2014
a_P	CheA autophosphorylation rate	12.5 s^{-1}	Frankel et al., 2014
a_B	Rate of CheB phosphorylation by CheA	15 μM^{-1} s^{-1}	Stewart, Jahreis, and Parkinson, 2000
d_B	CheB autodephosphorylation rate	0.5 s^{-1}	Stewart, 1993, Kentner and Sourjik, 2006
a_Y	Rate of CheY phosphorylation by CheA	50 μM^{-1} s^{-1}	Frankel et al., 2014
d_Z	Rate of CheY desphosphorylation by CheZ	5 μM^{-1} s^{-1}	Frankel et al., 2014
Motor Parameters			
Name	**Description**	**Value**	**Reference**
ω_0	Basal switching frequency	1.3 s^{-1}	Sneddon et al., 2012, Cluzel et al., 2000
$\varepsilon_{3,0}$	Motor steepness	80	Yuan et al., 2013, Dufour et al., 2014
K_D	Dissociation constant of CheY-motor interaction	3.06 μM	Sneddon et al., 2012, Cluzel et al., 2000
k_{on}	Rate of motor adaptation	0.025 s^{-1}	Dufour et al., 2014
$\varepsilon_{3,1}$	Slope of motor steepness response to change in bound FliM	1.96	Dufour et al., 2014
Δ_n	Effective half-max of FliM binding to the motor	4.16	Dufour et al., 2014
n_0	Number of FliM on the motor at rest	36	
n_1	Minimum number of FliM on the motor	34	Dufour et al., 2014
n_2	Maximum number of FliM on the motor	44	Dufour et al., 2014
Flagellar bundle parameters			
Name	**Description**	**Value**	**Reference**
λ	Mean waiting time of semi-coiled to curly transition	0.2 s	Sneddon et al., 2012
$N_{flagella}$	Total number of flagella per cell	4	Sneddon et al., 2012
N_{bundle}	Number of flagella rotating CCW to form a bundle	2	Sneddon et al., 2012
Gene expression parameters			
Name	**Description**	**Value**	**Reference**
T_{Tot}	Population mean receptors per cell (Tar + Tsr)	26000 mol./cell	Li and Hazelbauer, 2004
A_{Tot}	Population mean CheA proteins per cell	7700 mol./cell	Li and Hazelbauer, 2004
W_{Tot}	Population mean CheW proteins per cell	7200 mol./cell	Li and Hazelbauer, 2004
R_{Tot}	Population mean CheR proteins per cell	160 mol./cell	Li and Hazelbauer, 2004
B_{Tot}	Population mean CheB proteins per cell	270 mol./cell	Li and Hazelbauer, 2004
Y_{Tot}	Population mean CheY proteins per cell	6300 mol./cell	Li and Hazelbauer, 2004
Z_{Tot}	Population mean CheZ proteins per cell	2700 mol./cell	Li and Hazelbauer, 2004
x	Conversion between mol./cell and mM for proteins	833 μM/(mol./cell)	Frankel et al., 2014
A_{YZ}	Translational coupling coefficient between CheY and CheZ	0.25	Lovdok et al., 2009
η	Intrinsic noise scaling coefficient	0.0125	*this study*
ω	Extrinsic noise scaling coefficient	0.026	*this study*
Cell growth parameter			
Name	**Description**	**Value**	**Reference**
r	Cell generation time	1 h^{-1}	*this study*

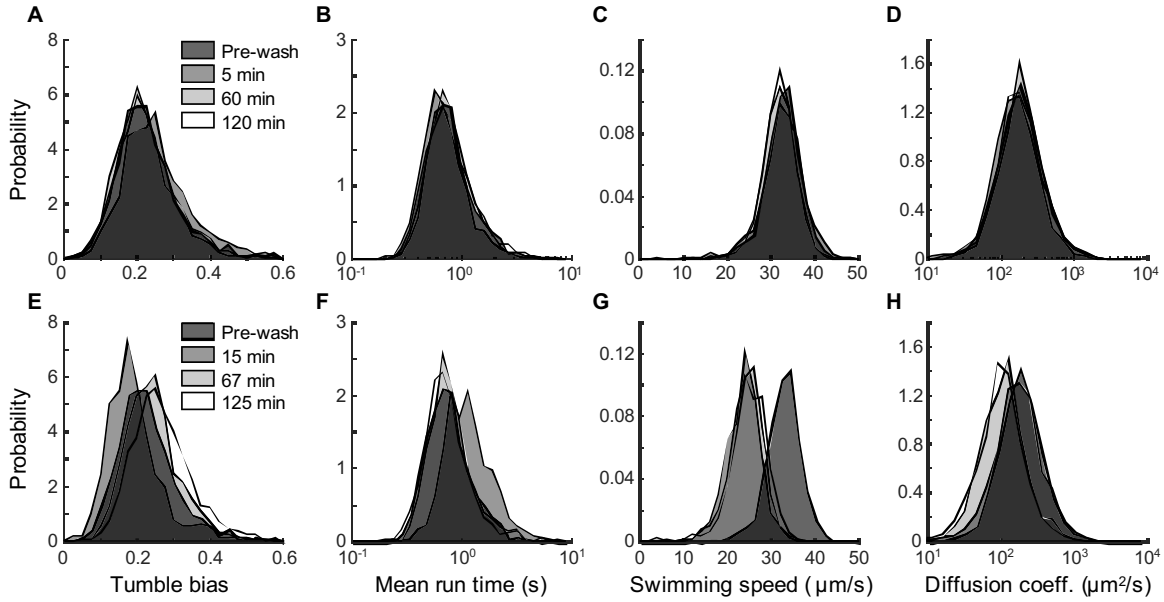

S1 Fig. Effect of the chemotaxis buffer, PEGDA, and LAP on the distributions of swimming phenotypes in a clonal *E. coli* RP437 population. (A-D) Probability distribution of cell tumble biases, mean run times, mean swimming speeds, and cell diffusion coefficients from cells swimming in chemotaxis buffer after the indicated incubation times. (E-H) Same distributions from cells swimming in chemotaxis buffer supplemented with 5% PEGDA and 0.05%LAP after the indicated incubation times.

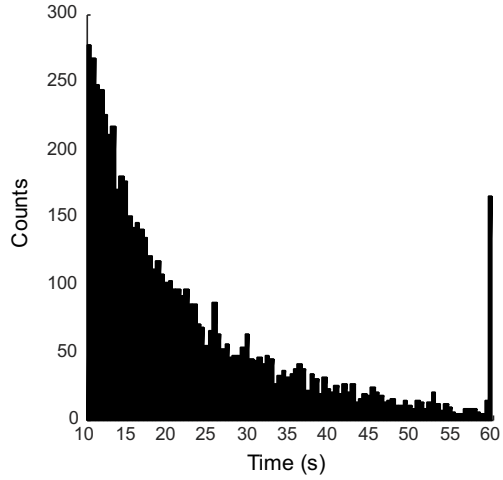

S2 Fig. Distribution of trajectory length obtained from tracking 6,332 individual swimming RP437 cells for 60 seconds.

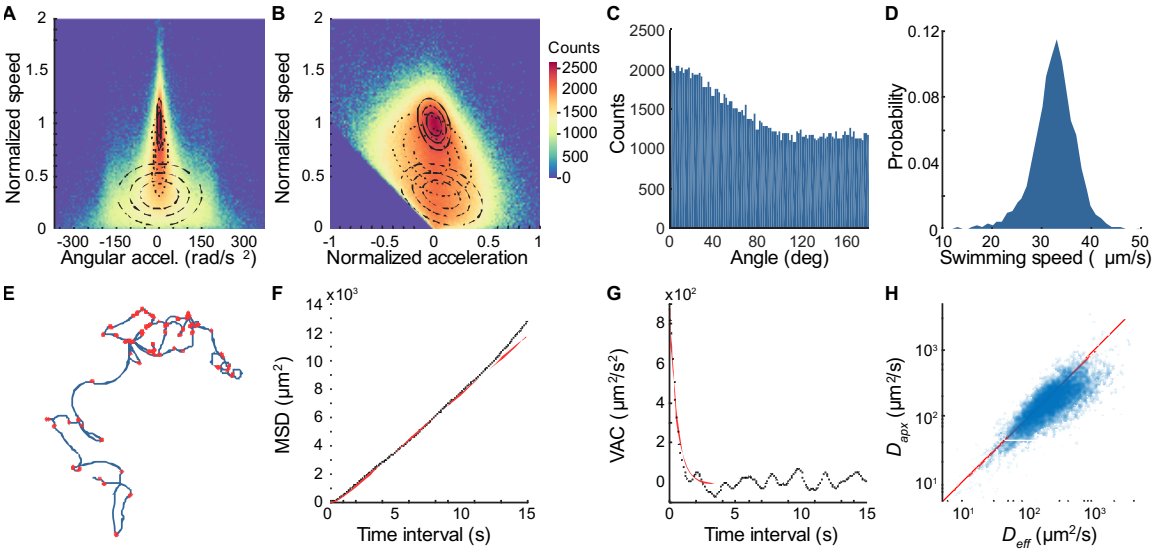

S3 Fig. Tumble detection and diffusion coefficient calculations. (A) Density plot of normalized cell swimming speed as a function of angular acceleration. (B) Density plot of normalized cell swimming speed as a function of normalized cell acceleration. The three-dimensional density distribution comprising ~6 millions data points was fitted with a mixture of three tri-variate Gaussian distributions to represent three possible cell swimming states: running (solid lines), tumbling (dashed lines), and intermediate (dotted lines). (C) Distribution of angles measured from the change in direction in the swimming trajectories after each detected tumble for RP437 cells. (D) Probability distribution the mean swimming speeds of individual cells. (E) Example of a 60 seconds single-cell trajectory where detected tumbles are marked with red dots. (F) Mean square displacement and (G) velocity auto-correlation as a function of time intervals calculated from a representative cell trajectory (black) with the corresponding fit (red) to extract the cell diffusion coefficient. (H) Scatter plot of the approximated diffusion coefficients (D_{apx}) calculated from the mean run time between tumbles against the effective diffusion coefficient (D_{eff}) calculated for the cell directional persistence for each cell. The distributions were calculated from about 6,000 individual trajectories combined from three independent experiments.

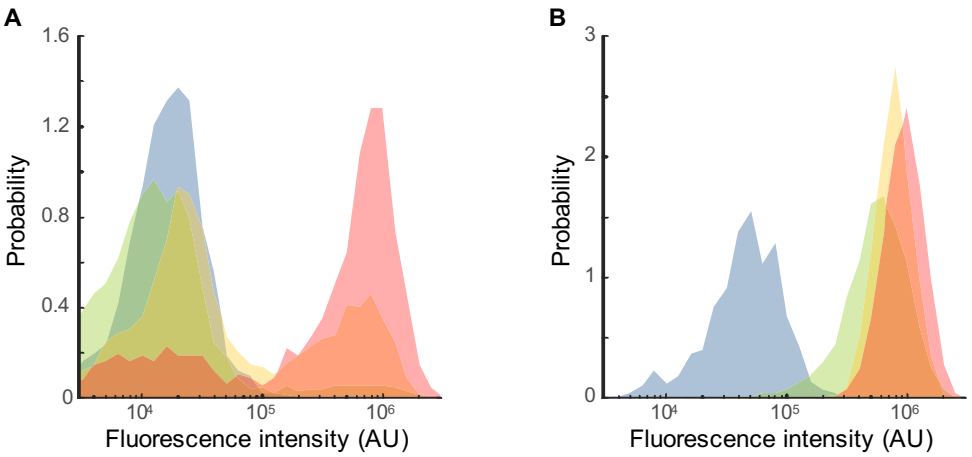

S4 Fig. Induction of fluorescently labeled chemotaxis proteins. (A) Probability distributions of fluorescence intensities from the inductions of CheB-mYFP in the YSD2073 mutant strain (pRha cheB-mYFP, pLac mCherry-cheR) with four rhamnose concentrations: 0 mM (cyan), 0.3 mM (green), 1 mM (yellow), and 3 mM (red). (B) Probability distributions of fluorescence intensities from the inductions of mCherry-CheR in the same strain with four IPTG concentrations: 0 µM (cyan), 10 µM (green), 30 µM (yellow), and 100 µM (red). The fluorescence intensities were obtained from the analysis of thousands of cells using MicrobeTracker on epi-fluorescence microscopy images. The bimodal distribution of fluorescence intensities from the expression of CheB-mYFP is a result of the bi-stability of the pRha promoter.

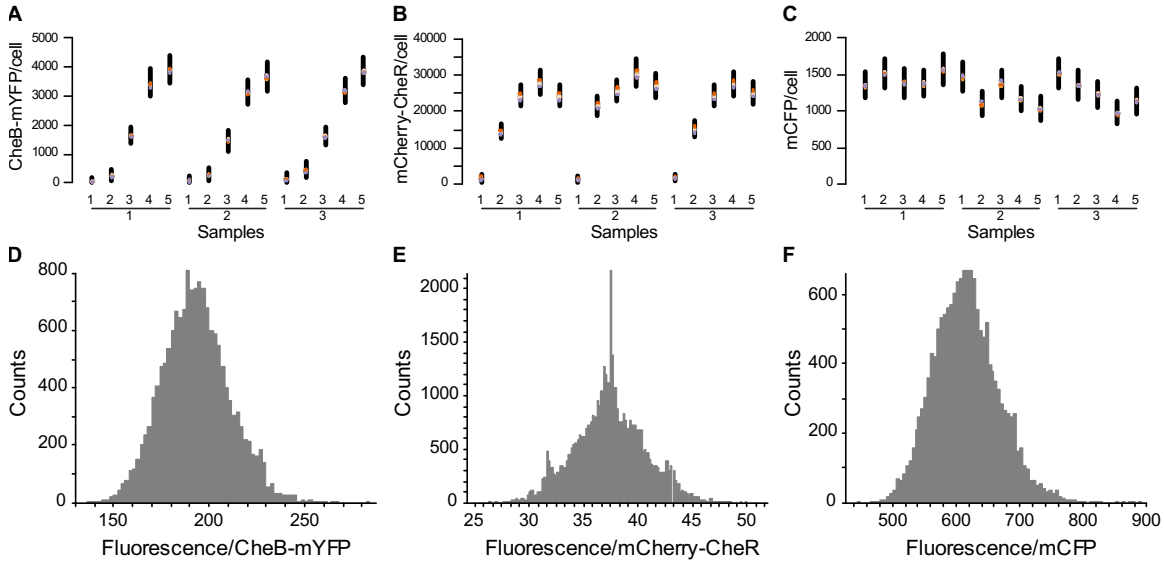

S5 Fig. Calibration of fluorescence units per fluorescent molecules using Bayesian regression analysis with the YSD2073 mutant strain (pRha cheB-mYFP, pLac mCherry-cheR, pBla mCFP). (A) Estimated numbers of CheB-mYFP molecules per cell as a result of induction with different rhamnose concentrations (1: 0 mM, 2: 0.3 mM, 3: 1 mM; 4: 3 mM, 5: 10 mM) shown for three independent experiments. The black lines represent the 80% confidence interval. The colored dots indicate the median for each of the 8 chains of the MCMC sampling. (B) Estimated numbers of mCherry-CheR molecules per cell as a result of induction with different IPTG concentrations (1: 0 µM, 2: 10 µM, 3: 30 µM; 4: 100 µM, 5: 1 mM) shown for three independent experiments. (C) Estimated numbers of mCFP molecules per cell as a result of induction with different IPTG concentrations (1: 0 µM, 2: 10 µM, 3: 30 µM; 4: 100 µM, 5: 1 mM) shown for three independent experiments. As expected mCFP expression does not respond to the presence of IPTG or rhamnose. (D) Posterior probability distribution of the expected number of fluorescence units per CheB-mYFP molecule. (E) Posterior probability distribution of the expected number of fluorescence units per mCherry-CheR molecule. (F) Posterior probability distribution of the expected number of fluorescence units per mCFP molecule.

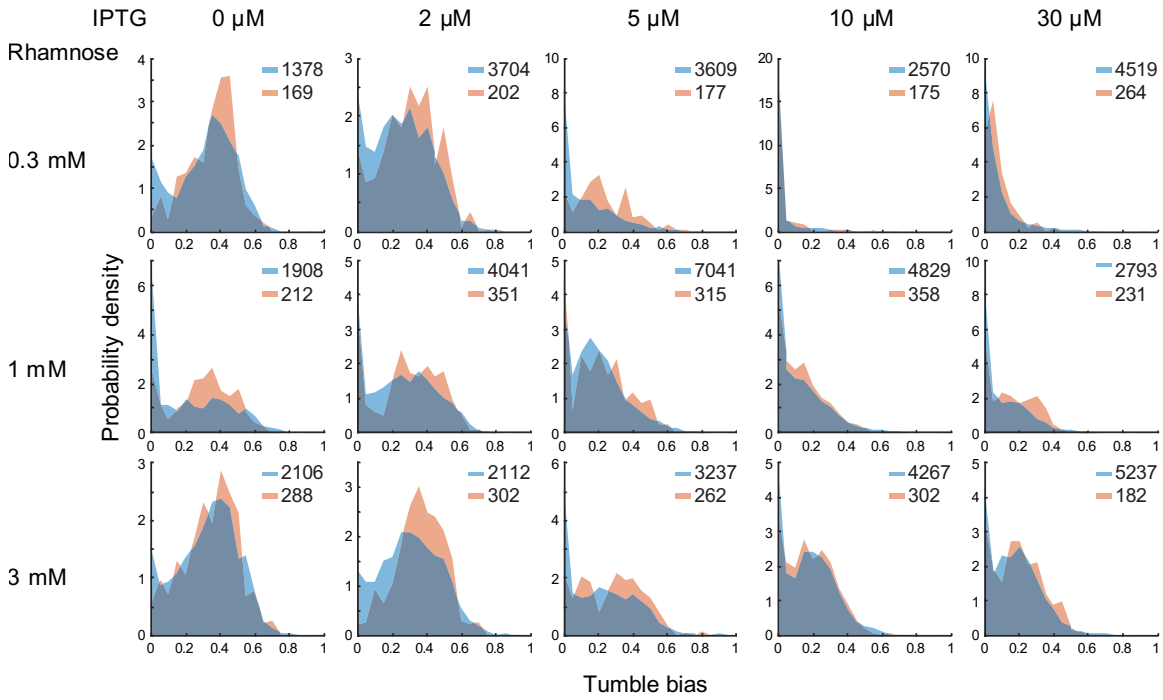

S6 Fig. Manipulating and sampling tumble bias distributions in a mutant *E. coli* strain expressing mCherry-CheR and CheB-mYFP. The YSD2072 mutant strain (pLac cheB-mYFP, pRha mCherry-cheR, pBla mCFP) was grown in M9 glycerol medium supplemented with the indicated concentrations of the inducers rhamnose and IPTG to obtain different distributions of tumble biases. The distributions of phenotypes from the population of cells trapped and imaged in the hydrogel (red) is comparable to the distribution of phenotypes from the entire cell population (blue) indicating that the trapped cells represent an unbiased sample of the population. The number of cells represented in each distribution is indicated for each plot.

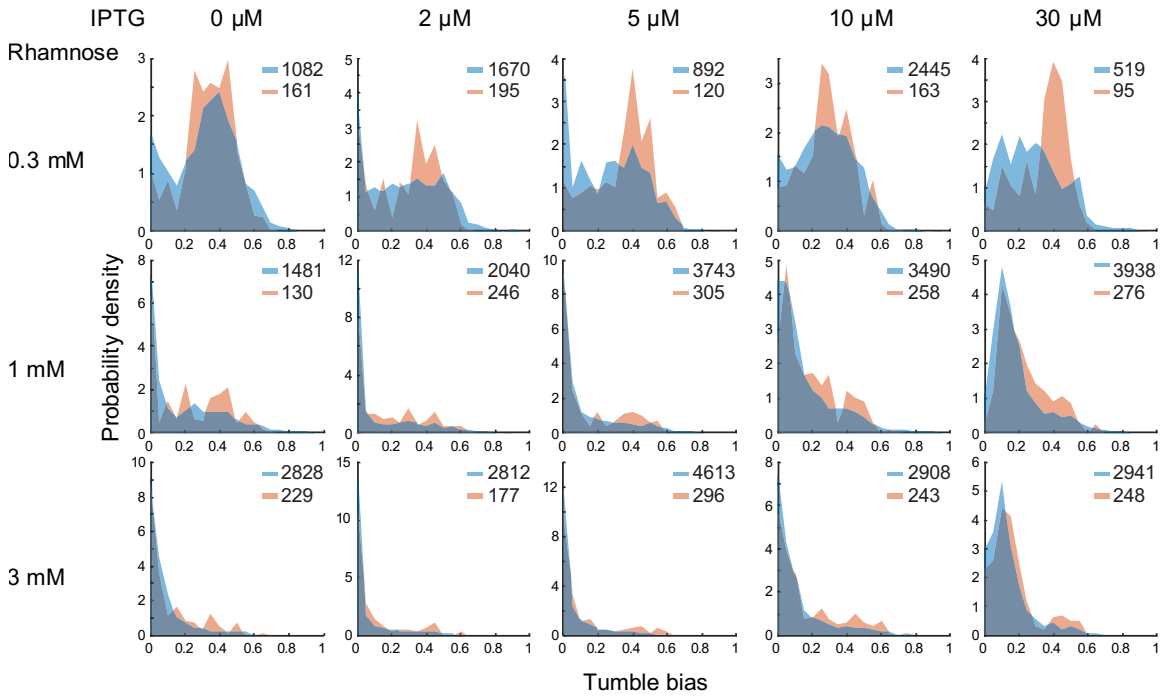

S7 Fig. Manipulating and sampling tumble bias distributions in a mutant *E. coli* strain expressing mCherry-CheR and CheB-mYFP. The YSD2073 mutant strain (pRha cheB-mYFP, pLac mCherry-cheR, pBla mCFP) was grown in M9 glycerol medium supplemented with the indicated concentrations of the inducers rhamnose and IPTG to obtain different distributions of tumble biases. The distributions of phenotypes from the population of cells trapped and imaged in the hydrogel (red) is comparable to the distribution of phenotypes from the entire cell population (blue) indicating that the trapped cells represent an unbiased sample of the population. The number of cells represented in each distribution is indicated for each plot.

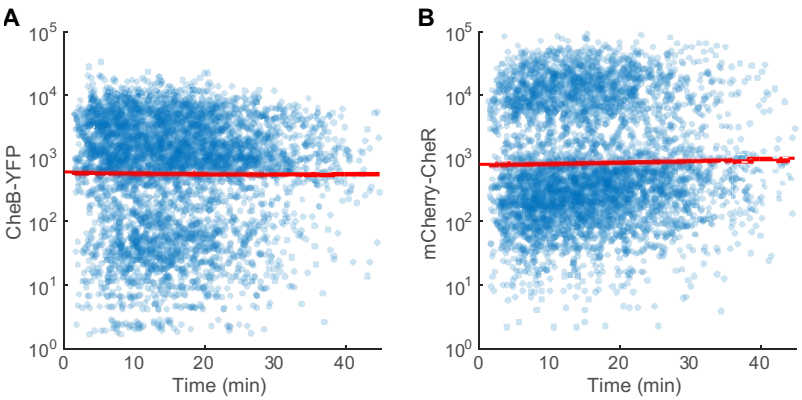

S8 Fig. Protein stability during single-cell fluorescence imaging of cells immobilized in the hydrogel. (A) Scatter plot of the estimated number of CheB-YFP proteins in each cell as a function of time after cell immobilization. A linear fit (red line) indicates that there is no significant change in protein numbers as a function of time (slope -0.0022 min^{-1}, 95% confidence interval [-0.0094; 0.0050]). (B) Scatter plot of the estimated number of mCherry-CheR proteins in each cell as a function of time after cell immobilization. A linear fit (red line) indicates that there is no significant change in protein numbers as a function of time (slope 0.0049 min^{-1}, 95% confidence interval [-0.0025; 0.0123]).

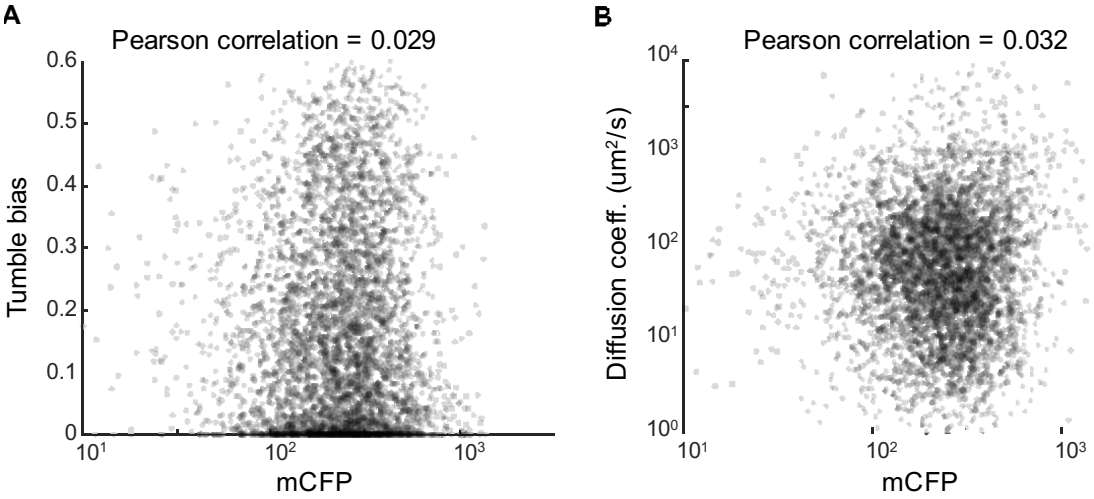

S9 Fig. Correlations of single-cell swimming phenotypes with mCFP numbers. (A) Scatter plot of single-cell tumble biases against mCFP numbers. (B) Scatter plot of single-cell diffusion coefficients against mCFP numbers.

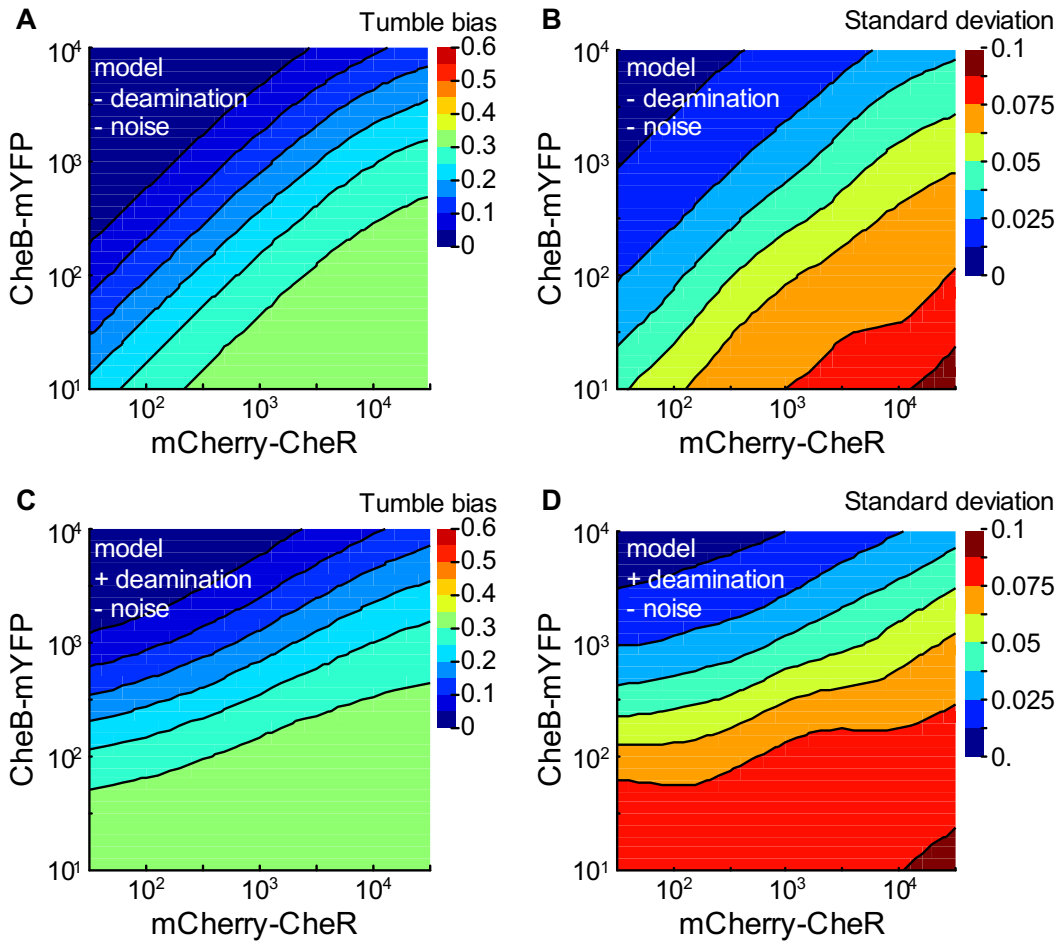

S10 Fig. Tumble bias and residual standard deviation as a function of CheR and CheB numbers predicted from a model missing CheB-dependent receptor deamidation and/or receptor adaptation noise. (A) Contour plot of the local linear regression of the predicted tumble bias as a function of CheR and CheB numbers for a model missing both CheB-dependent receptor deamidation and receptor adaptation noise. (B) Contour plot of the predicted residual tumble bias standard deviation resulting from stochastic expression of the chemotaxis proteins with no signaling noise from the receptor cluster. (C) Contour plot of the local linear regression of the predicted tumble bias as a function of CheR and CheB numbers for a model including the deamidation reaction but missing receptor adaptation noise. (D) Contour plot of the predicted residual tumble bias standard deviation resulting from stochastic expression of the chemotaxis proteins with no signaling noise from the receptor cluster. From the stochastic gene expression model, we sampled 8405 cells covering the full range of CheR and CheB expression levels. We then calculated the corresponding tumble bias for each individual cell using a model of bacterial chemotaxis that does not take into account CheB-dependent receptor deamidation or receptor adaptation noise. The local linear regressions were done using a bandwidth of 20% of the data points.

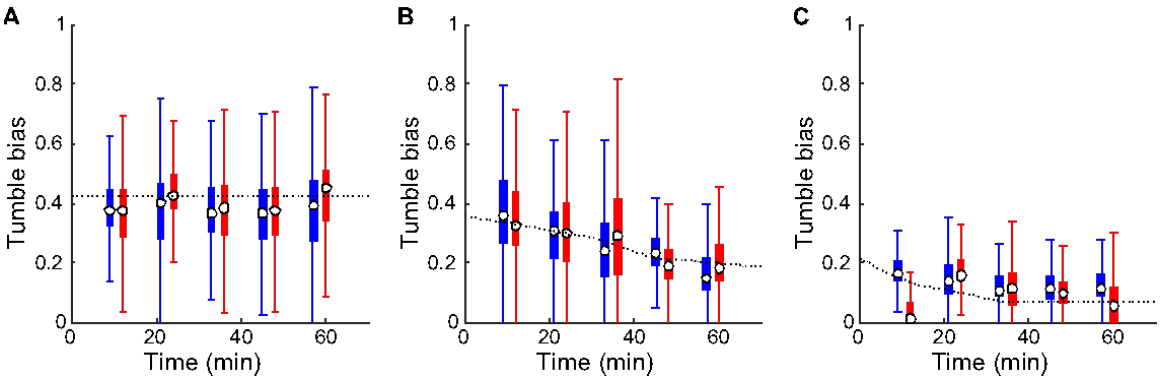

S11 Fig. Effect of CheB-YFP expression on the tumble bias in populations of motile cells. Box plots representing the evolution of the distributions of the tumble bias as a function of time of YSD2044 mutant cells grown (A) in the absence of inducer, (B) in the presence of 5 µM IPTG, or (C) in the presence of 50 µM IPTG, after the growth medium was exchanged with chemotaxis buffer. Two independent experimental trials are represented in red and blue. The white dots represent the medians. The boxes span the first and third quantiles. The whiskers indicate 1.5 times the interquartile range. The dotted lines represent the model predictions used to estimate the CheB-dependent deamidation rate (k_Q=0.64s^{-1}) and the number of expressed CheB proteins (0, 100, 250 molecules, respectively). The tumble bias trajectories were calculated over time by first solving the model at steady state with a cell doubling rate set to 1h^{-1} and then numerically solving the evolution of the differential equations after the doubling rate was set to 0 to simulate the transfer of cells from the growth medium to the chemotaxis buffer.

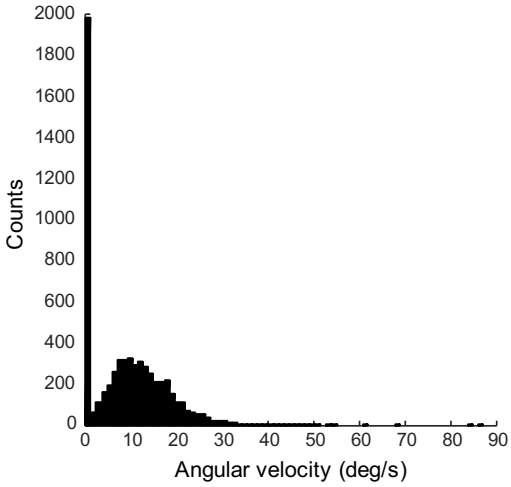

S12 Fig. Distribution of angular velocities extracted from the analysis of the mean square displacement and the velocity autocorrelation of each cell trajectory. The angular velocity is non-zero when cells swim close enough to the glass surface to be affected by hydrodynamic interactions between the glass and the cell body rotation.

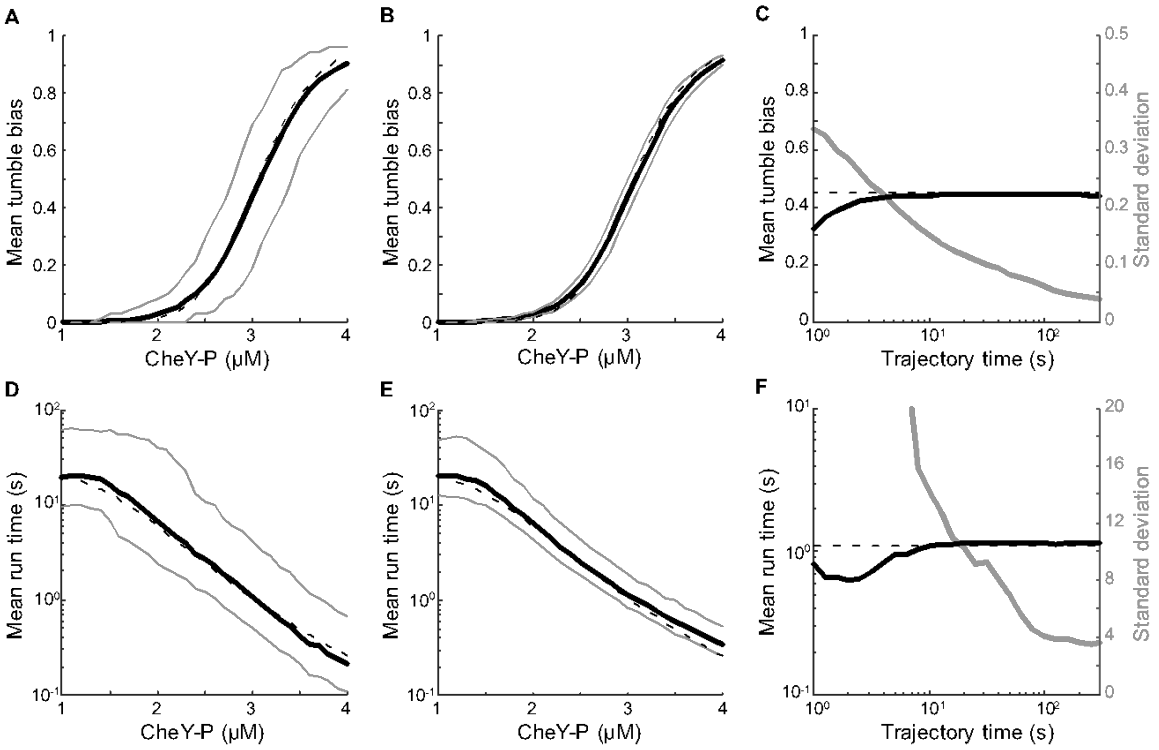

S13 Fig. Precision and accuracy of tumble detection on simulated swimming cell trajectories. (A) Mean cell tumble bias as a function of phosphorylated CheY (CheY-P) concentration for 10-second-long trajectories. The dashed line represents the expected theoretical relationship. The tumble detection algorithm was run on 1,000 simulated trajectories for each CheY-P concentrations. The solid line represents the mean of the calculated tumble biases. The grey lines delimit 90% of the probability density. (B) Same as A but for 300 seconds long trajectories. (C) Mean of the calculated tumble bias as a function of total simulation time. The trajectories of cells with 3 μM CheY-P were simulated for different amounts of time between 1 and 300 seconds. The dashed line represents the expected theoretical tumble bias. The tumble detection algorithm was run on 1,000 simulated trajectories for each simulation time. The solid line represents the mean of the calculated tumble biases. The grey line represents the standard deviation of the calculated tumble bias distribution. (D) Mean cell run time as a function of phosphorylated CheY concentration for 10-second-long trajectories. (E) Same as D but for 300 seconds long trajectories. (F) Mean of the calculated mean run time as a function of total simulation time.